

Segmentation of LG Enhanced Cardiac MRI

Kjersti Engan¹, Valery Naranjo², Trygve Eftestøl¹, Stein Ørn³ and Leik Woie³

¹University of Stavanger, Stavanger, Norway

²Labhuman, I3BH, Universitat Politècnica de València, Valencia, Spain

³Stavanger University Hospital, Stavanger, Norway

Keywords: Cardiac MRI, Segmentation, Late Gadolinium enhanced MRI.

Abstract: In this paper a method for segmentation of the endocardium in Late Gadolinium Enhanced Cardiac Magnetic Resonance (LGE-CMR) images is presented and combined with a previously proposed method for segmentation of the epicardium. The method is fully automatic and based on utilizing a priori knowledge about the type of images. No other image modalities, like CINE images, are used. Using a combination of a rough a priori model and preprocessed images, an a posteriori model is built. The final segmentation step is performed in the polar domain. We compare our results on a set of 395 images from 54 patients with segmentation using marker controlled watershed with different gradient images and different markers. The proposed method gives a mean Dice and Jaccard indices over all images as 0.85 and 0.74 respectively.

1 INTRODUCTION

Myocardial Infarction (MI) caused by cardiac ischemia is one of the major causes of death and disability in the world. MI is defined by pathology as myocardial cell death due to insufficient blood supply. Dead myocardial cells are replaced by myocardial scar (Thygesen et al., 2007). After MI it is important to evaluate the degree of damage. Cardiac Magnetic Resonance (CMR) imaging is a non-invasive method for evaluating the myocardium. To be able to distinguish the *scar*, i.e. the dead cells, from normal myocardial tissue, a gadolinium based contrast agent is most frequently used. Images that visualize dead tissue can be generated by the use of the late Gadolinium Enhancement Cardiac Magnetic Resonance (LGE-CMR) technique. This paper is addressing the problem of automatically segmenting the myocardium in LGE-CMR images of the left ventricle.

Healthy myocardium appears very dark in CMR images, however the edges of the heart in LGE-CMR images where the patient has a scar in the myocardium are sometimes very weak or non-existing since the scarred areas will take intensity levels close to the blood pool or the surrounding areas. This makes automatic segmentation of the myocardium in LGE-CMR images difficult. In many hospitals today the segmentation of the myocardial muscle is per-

formed manually or semi-automatically by expert cardiologists. This can be time-consuming work, and the results will have a degree of inter- and intra-observer variability.

1.1 Data Material

The Department of Cardiology at Stavanger University Hospital provided LGE-CMR images of 54 patients with varying number of slices, giving 395 images. All patients have had myocardial infarction prior to the examination, and 20 of them had profound scars and was later implanted with Implantable Cardioverter Defibrillator (ICD). CMR was performed using 1.5 T Philips Intera R 8.3, typical pixel size of $0.8 \times 0.8\text{mm}^2$, covering the whole ventricle with short-axis slices of 10 mm thickness, without interslice gaps. An example of all the 8 slices from one patient is seen in Figure 1, and the endocardium is the inner border of the dark ring (partly bright because of scar) approximately in the middle of each slice. All left ventricle, short axis view slices of all patients were manually segmented by expert cardiologists to provide a true marking. The true heart center used in some experiments refers to the centroid of the pixels in the myocardium extracted from these true endo- and epicardium markings.

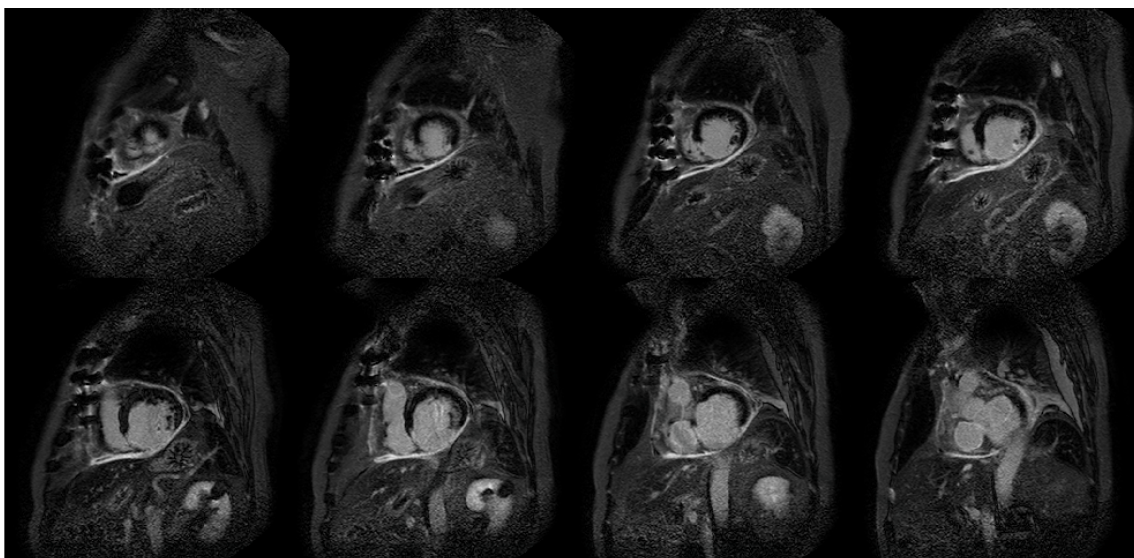


Figure 1: LGE-MRI slices of a patient with myocardial scar. Approximately at the middle of each slice there is an almost circular and brighter area which is the bloodpool of the heart. The myocardial muscle tissue surrounding the bloodpool is dark, and in a healthy subject it would have the appearance of a ring. In LGE-MRI, however, scarred tissue with reduced blood flow will appear brighter. Here we see that the myocardial muscle is partly as bright as the bloodpool because of infarction scar. The inner border of the myocardial muscle (the dark and partly bright ring) is the endocardium border. The outer border of the myocardial muscle is called the epicardium border.

1.2 Relation to Prior Work

There have been attempts to solve the problem of automatic segmentation reported in the literature. Some methods require manual input in the form of landmarks or cropping of region of interest, etc (de Bruijne and Nielsen, 2004; Spreeuwiers and Breeuwer, 2003; Heiberg et al., 2010). Others make use of additional data as the corresponding cine MR (ODonnell et al., 2003; Ciofolo et al., 2008; Wei et al., 2011; Wei et al., 2013), or a combination of cine images and some manual input (Dikici et al., 2004). However, the use cine-MR requires a suitable registration onto the LGE-CMR dataset, and this includes potential difficulties since patients position and holding of breath can introduce misalignments.

In our work all results are based solely on the LGE-CMR images. We presented a method for automatically finding the heart center in (Engan et al., 2013b) and segmentation of the *epicardium* (Engan et al., 2013a) with some early results. In this paper we have continued this work and are presenting a method for automatic segmentation of the *endocardium*. A *a priori* knowledge of typical heart size and shape is used as the input, and an *a posteriori* probability map is made iteratively. The final segmentation is based on the *a posteriori* probability maps, and information from all slices are taken into account. Recent work by Albà et.al. (Alba et al., 2012), (Alba et al., 2013) is

also based on the LE-CMR images alone without the need of cine MR sequences and corresponding registration. The 3D information and a conical model are utilized to detect initialization, somewhat similar to the way we find the heart center in (Engan et al., 2013b).

2 PROPOSED METHOD

The proposed method for segmentation of the myocardium is based on an iterative algorithm finding an *a posteriori probability map*, where the probability map can be interpreted as the probability of a specific pixel belonging to the myocardium. A block diagram of the complete system can be seen in Figure 2. The system starts by an algorithm for automatically finding the heart center from the whole LGE-CMR slices with no pre-cropping (block 1). This part will not be described here, but we proposed two algorithms for solving this problem in (Engan et al., 2013b). Using the heart center (HC) as input, an *a priori* model is made (block 2), and by using the iterative algorithm (block 3), an *a posteriori* probability model is found. This *a posteriori* model gives a good foundation for the last segmentation step of both the epicardium and the endocardium. The iterative algorithm of block 3 is important in the context of this paper, thus described

here. However a version of this was presented in (Engan et al., 2013a) together with some early results on segmenting the *epicardium* (block 4). The main focus of this paper is block 5, *segmentation of the endocardium*. The algorithm is shown and some results comparing with watershed segmentation of the blood-pool is presented in the results section.

In the following, let $f^i(\mathbf{x})$, $i = 1 \dots N_{slice}$ represent the left ventricle short axis LGE-CMR images of a patient. $\mathbf{x} = [x_{row} \ x_{column}]^T$ is the pixel position, and i represents the slice number.

2.1 Probability Map

The LGE-CMR images are hard to segment because the scars are bright, whereas the muscle is dark, the scars have similar intensity levels as the blood pool inside the endocardium border, and the edges are some places non-existing. The reason why an expert cardiologist is capable of segmenting the images manually is that the cardiologist will automatically use prior information of typical shapes and sizes of a heart. In the left ventricle short axis view the myocardium will more or less have the shape of a ring, and this information has to be utilized.

We propose to use a rough *a priori* model of the myocardium around the heart center for each slice imposed as a gaussian in the polar domain with the heart center as the origin for all angles. μ of the gaussian prior will correspond to the approximated radius at the middle of the myocardium for that slice, and is varied with the slice number. Typical values are found from a training set, but a large variance is used in the gaussian prior to make the *a priori* model robust. After mapping to cartesian coordinates and scaling all pixels to be within $[0, 1]$, this gives an *a priori* probability map, where the probability is seen as the probability for being a pixel in the myocardium.

Using the *a priori* probability model as input, we propose an iterative approach to refine the model and make an *a posteriori* probability map for the myocardium. At each iteration the probability model is combined with the inverse of the original (preprocessed) slices, a low pass filtering over the neighboring slices is performed, and the output is a new probability model. The inverse of the original is used because the myocardial muscle we want to segment appears dark in the images, and thus appears bright with high values in the inverse. The algorithm is depicted in Algorithm 1, and a brief explanation follows.

In line (3) of Algorithm 1, a morphological noise removal of the original slices, f^i is conducted using the morphological center, as defined in (Soille, 2003), and the structuring element B_{mc} as a square of size

Algorithm 1: Iterative probability map algorithm.

Data: CMR images $f^i(\mathbf{x}) \in \mathcal{R}^{N \times M}$, Prior prob.

map $p_0^i(\mathbf{x}) \in \mathcal{R}^{N \times M}$ $i = 1, \dots, N_{slice}$,

Result: Posteriori prob. map,

$p_{post}^i(\mathbf{x}) \in \mathcal{R}^{N \times M}$, $i = 1, \dots, N_{slice}$

```

1 initialization:  $k_{final}$ ;
2 for  $i \leftarrow 1$  to  $N_{slice}$  do
3    $f_{prep}^i(\mathbf{x}) \leftarrow \beta_{B_{mc}}(f^i)$ ;
4    $f_{inv}^i(\mathbf{x}) = \text{scale}(\text{ones}(N, M) - f_{prep}^i(\mathbf{x}))$ ;
5 end
6 for  $k \leftarrow 0$  to  $k_{final} - 1$  do
7    $f_{temp}(\mathbf{x}) = p_k(\mathbf{x}) \times f_{inv}(\mathbf{x})$ ;
8    $f_{temp}(\mathbf{x}) \leftarrow LPfiltZ(f_{temp}(\mathbf{x}))$ ;
9    $p_{k+1}(\mathbf{x}) \leftarrow \text{scale}(f_{temp}(\mathbf{x}))$ ;
10 end
11  $p_{nof}(\mathbf{x}) = p_0(\mathbf{x}) \times (f_{inv}(\mathbf{x}))^{k_{final}}$ ;
12  $p_{post}(\mathbf{x}) =$ 
    $\text{scale}(w_1 p_{k_{final}}(\mathbf{x}) + (1 - w_1) p_{nof}(\mathbf{x}))$ ;
13 return( $p_{post}$ );
```

3×3 pixels. The noise removal results in a preprocessed slice, $f_{prep}^i(\mathbf{x})$, and the inverse of the preprocessed slice is found in line (4) as $f_{inv}^i(\mathbf{x})$. The main iteration is done in line 6-10, using the previous probability map, $f_{temp}(\mathbf{x}) = p_k(\mathbf{x}) \times f_{inv}(\mathbf{x})$, Low Pass (LP) filtering over the slices, $LPfiltZ(f_{temp}(\mathbf{x}))$, and subsequently finding a new probability map, $p_{k+1}(\mathbf{x})$ by scaling the result of the filtering. Another map is found without filtering over the slices, $p_{nof}(\mathbf{x})$, directly without any iterations as (line 11): $p_{nof}(\mathbf{x}) = p_0(\mathbf{x}) \times (f_{inv}(\mathbf{x}))^{k_{final}}$. The final probability model is a scaled and weighted sum (line 12) between $p_{k_{final}}(\mathbf{x})$ and $p_{nof}(\mathbf{x})$. $A \times B$ denotes the Hademard product.

In Figure 3 an example patient is depicted. Top two rows show the *a priori* probability map, middle rows show the *a posteriori* probability map, and last two rows shows the original images for this patient.

2.2 Segmentation

The *a posteriori* probability map looks promising, but still the segmentation is challenging. The scarred areas might appear quite dark in the probability images, thus the probability values can differ significantly at different angles. Consequently, a global thresholding technique will not work, regardless of the chosen threshold. The heart center at each slice, HC_i is an important input, and from the heart center the probability values at all radii are evaluated at different angles, $\theta \in [0, 2\pi]$ for both epicardium and

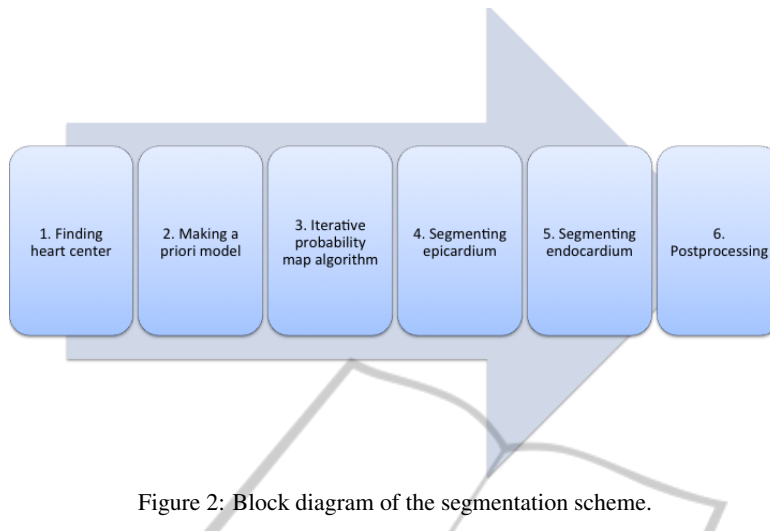


Figure 2: Block diagram of the segmentation scheme.

endocardium segmentation. Since we know that the endocardium borders lie within the epicardium borders, we start by finding the epicardium mask and use that as an input for the endocardium segmentation.

The algorithm for segmenting the epicardium was presented and explained in (Engan et al., 2013a) and will not be repeated here. In short, the epicardium segmentation algorithm uses the *a posteriori* probability map as well as the heart centers as input. A morphological closed-hole preprocessing of the probability map is done prior to a Otsu's multilevel thresholding. Using the heart center position in each slice, HC_i , as origin, the values after the multilevel thresholding are interpreted in polar coordinates giving $R_v(\theta, r)$, where θ is the angle and r the radius. The partial derivative of $R_v(\theta, r)$ with respect to r is found for all θ , $D_r(\theta, r)$, and the first negative value of the derivative (smallest radius) is marked as a candidate epicardium border point, $R_{epi}^i(\theta)$, for each θ . Some final steps are dealing with angles with missing candidate points by looking at neighboring angles and slices.

The proposed segmentation of the endocardium is also based on the *a posteriori* probability map, $p_{post}^i(\mathbf{x}) \in \mathcal{R}^{N \times M}$, $i = 1, \dots, N_{slice}$. The segmentation of the epicardium is executed first, and a resulting epicardium mask, $Mask_{epicard}^i(\mathbf{x})$, is used as additional information since the endocardium must lie inside the epicardium. A pseudocode of the algorithms for endocardium segmentation based on the probability maps is seen in Algorithm 2, and an explanation follows:

A multilevel version of Otsu's method (Otsu, 1979) is used for non uniformly quantizing of $p_{post}^i(\mathbf{x})$ into L levels: $f_q^i(\mathbf{x}) = Quant_{nonuni}^i(p_{post}^i(\mathbf{x}), L)$ (line 3). In line 4, the Hademar product between the quantized probability images and the epicardium mask sets

$f_{qepi}^i(\mathbf{x})$ to zero outside the epicardium.

Thereafter a conversion to polar coordinates with the heart center as the origin is performed giving $R_v(\theta, r)$. For each angle a candidate endocardium point is looked for as seen in line 7.

Let $R_v(\theta, 0)$ denote the value at the HC (heart center) point. If there exist points in $R_v(\theta, r)$ with value $R_v(\theta, r_1) > R_v(\theta, 0) + 1$, and r_{l_1} is the point closest to HC, then $R_{endo}(\theta) = r_{l_1}$. If not, there might exist points with value $R_v(\theta, r_m) > R_v(\theta, 0)$, and let r_{m_1} be the point closest to HC, then $R_{endo}(\theta) = r_{m_1}$. If neither of these points exists there are no candidate point for that specific angle at slice i .

If an angle, θ_k , is without candidate points for slice i , the other slices are checked to see if there exist any candidate points for θ_k (line 13-15). If any of the other slices have candidate points for θ_k , the one corresponding to the slice closest to slice i is chosen for slice i as well. If there are no candidate points for θ_k for any slices, the smallest $\Delta\theta$ to an angle with a candidate point is found within slice i , approximating the candidate point for θ_k using the same $R_{endo}(\theta_k + \Delta\theta)$ (line 16-18). Finally the convex hull of all candidate points is found as the endocardium mask, $Mask_{endocard}^i(\mathbf{x})$ (line 22).

2.3 Postprocessing

The endocardium mask $Mask_{endocard}^i(\mathbf{x})$ over the slices $i = 1, \dots, N_{slice}$ are compared. If there are segments that are only present in $Mask_{endocard}^k(\mathbf{x})$ it is considered a mistake, and removed from $Mask_{endocard}^k(\mathbf{x})$. If there are segments present in all slices except $Mask_{endocard}^j(\mathbf{x})$, this segment is added to $Mask_{endocard}^j(\mathbf{x})$. After finding the endocardium mask, the perimeter is calculated. Thereafter

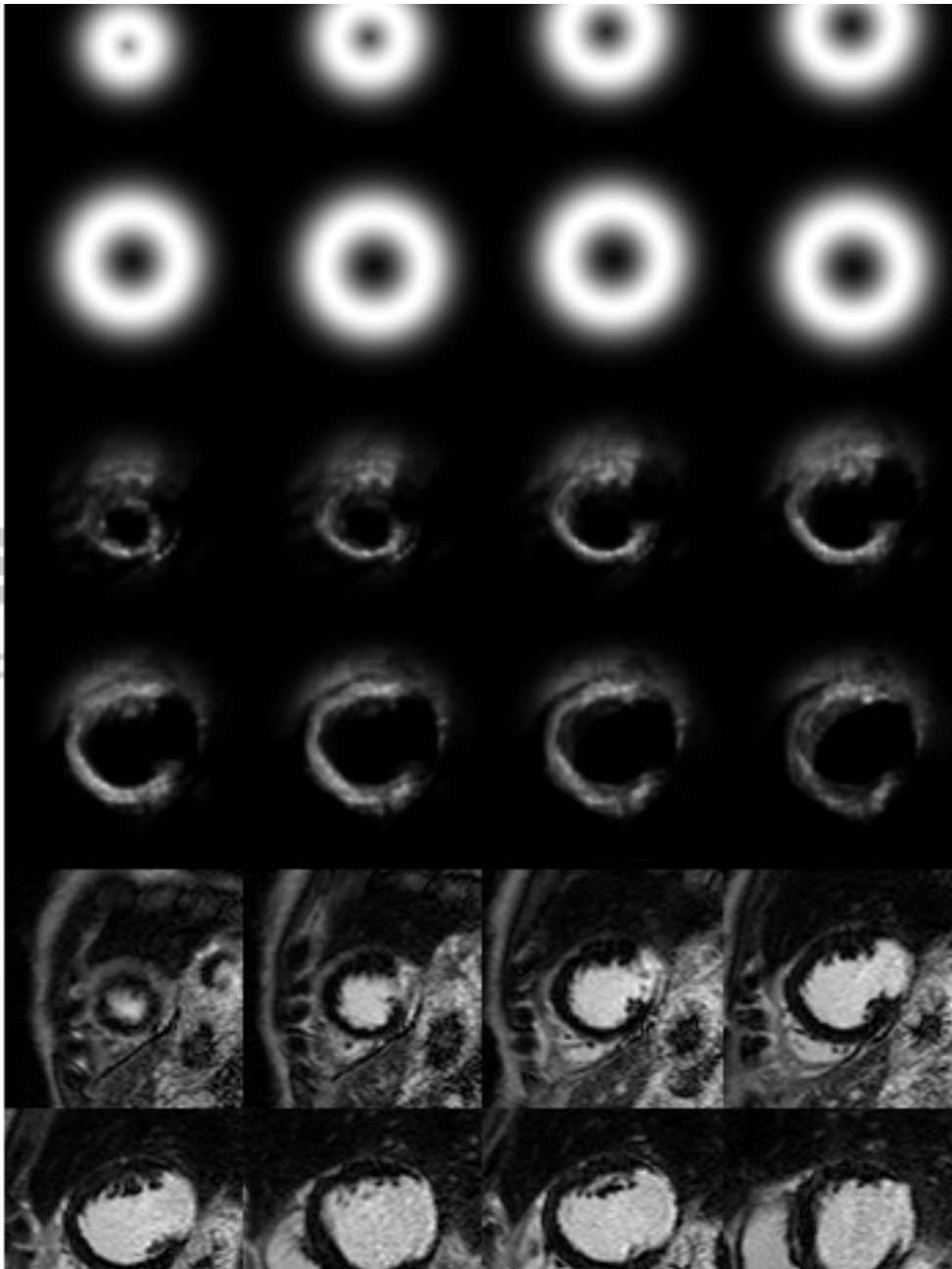


Figure 3: Top two rows, a priori probability map, second two rows, a posteriori probability map after 8 iterations, last two rows, original images.

a Fourier Descriptor (FD) (Impedovo et al., 1978) of this perimeter is found. The FD is lowpass filtered resulting in a smoother perimeter and a new mask.

3 EXPERIMENTS AND RESULTS

Segmentation experiments are performed on the set of 54 patients, 395 images. Different number of levels,

L , in the multilevel version of Otsus method in Algorithm 2 were tested in preliminary experiments. $L=4$ seemed to perform best and is used in the experiments presented here. The number of iterations of the iterative probability map scheme was set to 8. Results are presented as Dice (Dice, 1945) and Jaccard (Jaccard, 1912) indices.

The mean and standard deviation of the resulting Dice and Jaccard indices of the endocardium segmen-

Algorithm 2: Radial Segmentation of endocardium.

Data: CMR images $f^i(\mathbf{x}) \in \mathcal{R}^{N \times M}$, Posteriori prob. map, $p_{post}^i(\mathbf{x}) \in \mathcal{R}^{N \times M}, i = 1, \dots, N_{slice}$, heart center coordinates $HC_i, Mask_{epicard}^i(\mathbf{x})$;
Result: $Mask_{endocard}^i(\mathbf{x})$

```

1 initialization:  $R_{endo}^i(\theta) = 0, \theta \in [0, 2\pi]$ ;
2 for  $i = 1$  to  $N_{slice}$  do
3    $f_q^i(\mathbf{x}) = Quant_{nonuni}^i(p_{post}^i(\mathbf{x}), L)$ ;
4    $f_{qepi}^i(\mathbf{x}) = f_q^i(\mathbf{x}) \times Mask_{epicard}^i(\mathbf{x})$ ;
5   for  $\theta = 0$  to  $2\pi$  do
6      $R_v(\theta, r) = cart2poly(f_{qepi}^i(\mathbf{x}), \theta, HC_i)$ ;
7      $R_{endo}(\theta) = argmax(argmin_r[R_v(\theta, r) > (R_v(\theta, 0) + 1)], argmin_r[R_v(\theta, r) > R_v(\theta, 0)])$ ;
8   end
9    $R_{endo}^i(\theta) \leftarrow smooth(R_{endo}^i(\theta))$ ;
10 end
11 for  $i = 1$  to  $N_{slice}$  do
12   for  $\theta = 0$  to  $2\pi$  do
13     if  $R_{endo}^i(\theta) = 0$  then
14        $R_{endo}^i(\theta) \leftarrow mean(R_{endo}^j(\theta) \neq 0)$ 
15     end
16     if  $R_{endo}^i(\theta) = 0$  then
17        $R_{endo}^i(\theta) \leftarrow min_{|\Delta\theta|} (R_{endo}^i(\theta - \Delta\theta) \neq 0)$ 
18     end
19      $\mathbf{x}_\theta^i = poly2cart(R_{endo}^i(\theta))$ ;
20      $f_p^i(\mathbf{x}_\theta^i) = 1$ ;
21   end
22    $Mask_{endocard}^i(\mathbf{x}) = ConvexHull(f_p^i(\mathbf{x}))$ ;
23 end
24 return( $Mask_{endocard}(\mathbf{x})$ );
    
```

tation are seen in Table 2 where the automatic method for finding the heart center is used. In Table 3 the results from the same experiments, but using the true heart center as input, are shown. In Table 1 the mean and standard deviation of Dice index of both the *endocardium* and *epicardium* over all the images are

Table 1: Results for segmentation of endocardium and epicardium. Dice index, averaged over 395 images. Standard deviation in parentheses.

	Endocard Dice	Epicard Dice
True HC	0.87 (0.040)	0.90 (0.034)
Automatic HC	0.85 (0.048)	0.88 (0.046)

shown comparing results using the true heart center with the automatically found heart center. Two slices of an example patients are seen in detail in Figure 4 for illustration.

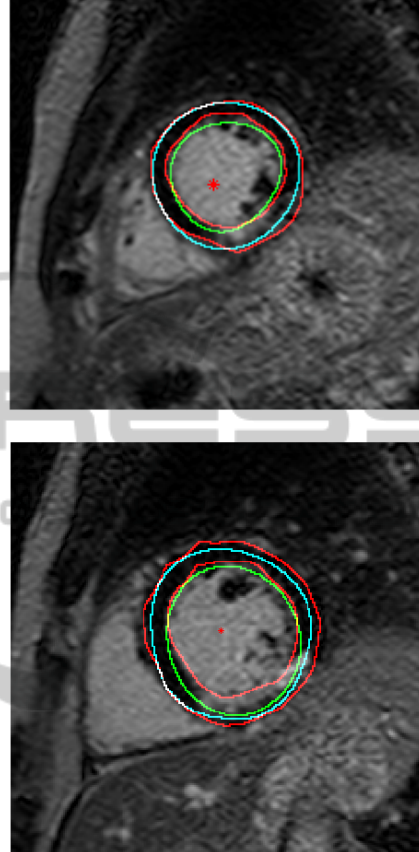


Figure 4: Segmentation results from two slices of an example patient. manual marking performed by cardiologist in red, automatically found heart center marked as red stars, epicardium contours in cyan, and endocardium contours in green. The top slice shows well performing segmentation. In the bottom slice the epicardium is segmented well, but the segmentation of the endocardium fails to include the scar in the myocardium

3.1 Comparison with Watershed Segmentation

To compare the proposed method with a classical and successful segmentation algorithm, we have compared with marker controlled watershed (Meyer, 1994; Soille, 2003) using different gradient images, and different markers.

Watershed segmentation was conducted using a morphological gradient on the CMR-images after some noise reduction was performed by using the

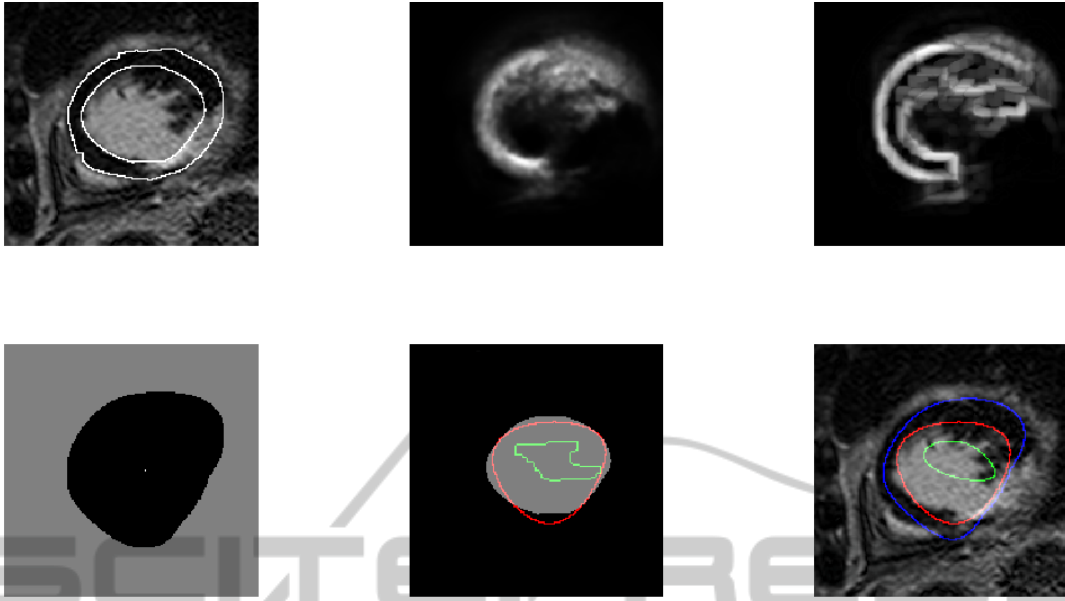


Figure 5: Segmentation results from one slice of an example patient. First row, left to right: Original image with manual markings, a posteriori probability map, gradient from a posteriori probability map. Second row, left to right: epicardium mask from automatic method used as external marker, true endocardium mask with proposed method in red and WS_{PMGepi} in green, original image with overlaid contours of epicardium (blue) endocardium (proposed method, red) and WS_{PMGepi} (green) after post processing.

morphological center algorithm (Soille, 2003). The corresponding results are named WS_{MG} when the external marker was the edge of the cropped image, where the cropping was done automatically using the heart center as input, and WS_{MGepi} when the external marker is defined by the epicardium mask, $Mask_{epicard}^i(\mathbf{x})$. The latter is done since the endocardium border cannot cross the (true) epicardium border.

Watershed segmentation using the *a posteriori* probability map images as input to find the morphological gradient images was also executed. The results are named WS_{PMG} when the external marker is the edge of the cropped image, and WS_{PMGepi} when the external marker is defined by the epicardium mask, $Mask_{epicard}^i(\mathbf{x})$. Two different internal marker are tested; the heart center from our proposed automatic method using the circular Hough Transform (CHT), see Table 2, and the true heart center, see Table 3.

Results from some slices of an example patient are depicted in Figure 6. For this example patient we can see that the proposed method performs better than the depicted WS_{MGepi} , since the latter includes more of the scar in the bloodpool. One slice of another example patient is depicted in Figure 5 at different stages together with the result of the proposed method as well as WS_{PMGepi} . In this example the WS_{PMGepi}

Table 2: Jaccard and Dice index, averaged over 395 images. Standard deviation in parentheses. Heart center from automatic method.

Endocard seg.	Dice	Jaccard
Prop.method	0.85 (0.048)	0.74 (0.070)
WS_{MG}	0.80 (0.075)	0.68 (0.099)
WS_{MGepi}	0.83 (0.060)	0.71 (0.084)
WS_{PMG}	0.78 (0.050)	0.65 (0.068)
WS_{PMGepi}	0.79 (0.066)	0.65 (0.086)

Table 3: Jaccard and Dice index averaged over 395 images. True heart center (HC) as input.

Endocard seg.	Dice	Jaccard
Prop.method	0.87 (0.040)	0.77 (0.062)
WS_{MG}	0.80 (0.075)	0.68 (0.099)
WS_{MGepi}	0.84 (0.055)	0.72 (0.080)
WS_{PMG}	0.80 (0.055)	0.67 (0.075)
WS_{PMGepi}	0.81 (0.068)	0.69 (0.088)

fails completely whereas the proposed method performs quite well.

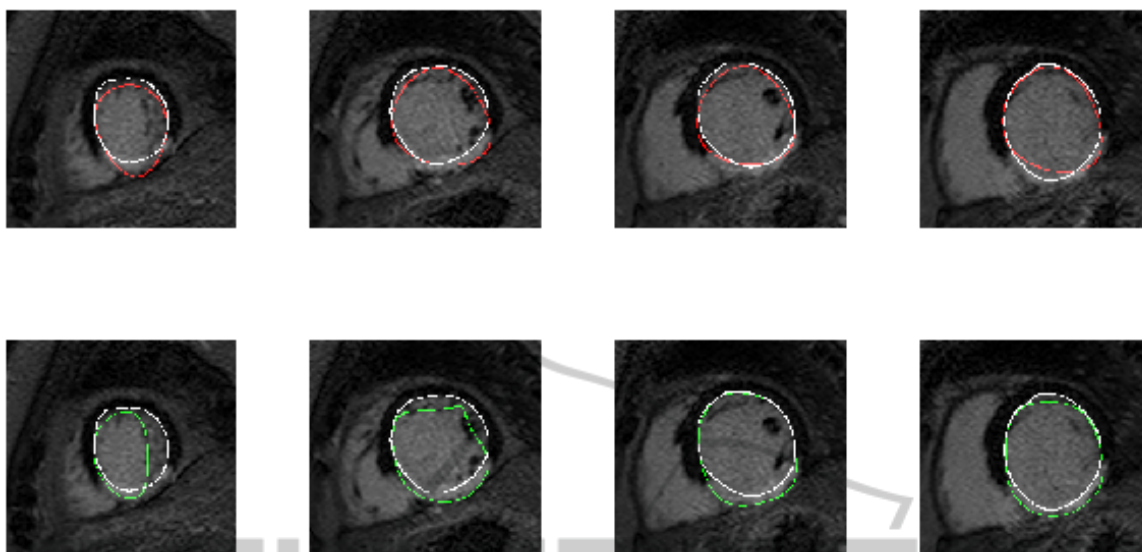


Figure 6: Segmentation results from some slices of an example patient. First row, white is manual marking, red is result from proposed method, dice index of this patient is 0.90. Second row, white is manual marking, green is WS_{MGepi} . Dice index of this patient is 0.84.

4 CONCLUSION

The presented method for segmentation of endocardium in LGE-CMR completes a larger system for automatic segmentation of the myocardium in LGE-CMR. The proposed system is based on using some prior information about LGE-CMR images: the bloodpool and the myocardial muscle is approximately circular and this is used when constructing an a priori probability map. The 3D information is utilized both finding the heart center and when producing the a posteriori probability map. The CMR images are not *true 3D* in the sense that the resolution in the z-direction (i.e. between slices) is much coarser than the resolution within a slice.

All experiments are conducted on a dataset of 54 patients, all with myocardial infarctions. Twenty of these patients are patients implanted with ICD (CMR images recorded prior to implantation), and these patients have severe scars, and sometimes enlarged hearts, making the segmentation even more challenging.

Results on the endocardium segmentation using the proposed method was compared to results using watershed with different gradients and different external markers. The mean Dice and Jaccard of the proposed fully automatic method are 0.85 and 0.74 respectively. Using the true heart center as input improves the Dice index to 0.87 and the Jaccard index to 0.77 showing the potential of the latter part of the proposed system. Watershed gave the corresponding

results 0.8 and 0.68. Using the epicardium segments from the proposed method as the external marker improved the watershed results, were the best results gave Dice index 0.83 and Jaccard index 0.71. The reported results in (Alba et al., 2012) are very good (Mean Dice index of 0.81 for the myocardial muscle), but on a limited dataset of LGE-CMR images (20 patients). In future work we will strive to do a fair comparison of our method with (Alba et al., 2013).

REFERENCES

- Alba, X., i Ventura, R. F., Lekadir, K., and Frangi, A. (2012). Conical deformable model for myocardial segmentation in late-enhanced MRI. In *Proceedings of IEEE International Symposium on Biomedical Imaging (ISBI)*. 10.1109/ISBI.2012.6235536.
- Alba, X., i Ventura, R. F., Lekadir, K., Tobon-Gomez, C., Hoogendoorn, C., and Frangi, A. (2013). Automatic cardiac lv segmentation in MRI using modified graph cuts with smoothness and interslice constraints. *Magnetic Resonance in Medicine*. doi: 10.1002/mrm.25079.
- Ciofolo, C., Fradkin, M., Mory, B., Hautvast, G., and Breeuwer, M. (2008). Automatic myocardium segmentation in late-enhancement MRI. In *Proceedings of IEEE International Symposium on Biomedical Imaging (ISBI)*.
- de Bruijne, M. and Nielsen, M. (2004). Shape particle filtering for image segmentation. In *Proc. of MICCAI*, volume 3216, pages 168–175.
- Dice, L. R. (1945). Measures of the amount of ecologic

- association between species. *Ecology*, 26(3):297–302. doi:10.2307/1932409.
- Dikici, E., O'Donnell, T., Setser, R., and White, R. (2004). Quantification of delayed enhancement MR images. In *Proceedings of the International Conference on Medical Image Computing and Computer-Assisted Intervention*, pages 250–257.
- Engan, K., Naranjo, V., Eftestøl, T., Ørn, S., and Woie, L. (2013a). Automatic segmentation of the epicardium in late gadolinium enhanced cardiac MR images. In *Proc. of Comp. in Cardiology 2013*, Zaragoza, Spain.
- Engan, K., Naranjo, V., Eftestøl, T., Woie, L., Schuchter, A., and Ørn, S. (2013b). Automatic detection of heart center in late gadolinium enhanced MRI. In *Proceedings of MEDICON 2013*, Sevilla, Spain.
- Heiberg, E., Sjgren, J., Ugander, M., Carlsson, M., Engblom, H., and Arheden, H. (2010). Design and validation of segment a freely available software for cardiovascular image analysis. In *BMC Medical Imaging*, volume 10:1.
- Impedovo, S., Marangelli, B., and Fanelli, A. M. (1978). A fourier descriptor set for recognizing nonstylized numerals. *IEEE Trans. Sys., Man., Cyber*, 8(8):640–645. doi: 10.1109/TSMC.1978.4310042.
- Jaccard, P. (1912). The distribution of the flora in the alpine zone. *New Phytologist*, (11):37–50.
- Meyer, F. (1994). Topographic distance and watershed lines. *Signal Processing*, 38:113–125.
- O'Donnell, T., Xu, N., Setser, R., and White, R. (2003). Semi-automatic segmentation of nonviable cardiac tissue using cine and delayed enhancement magnetic resonance images. In *Proceedings of SPIE 2003*, volume 5031, page 242.
- Otsu, N. (1979). A threshold selection method from gray-level histograms. *IEEE Trans. Sys., Man., Cyber*, 9(1):62–66. doi:10.1109/TSMC.1979.4310076.
- Soille, P. (2003). *Morphological Image Analysis*. Springer-Verlag, Berlin Heidelberg, Germany, 2 edition.
- Spreeuwens, L. and Breeuwer, M. (2003). Detection of left ventricular and epi- and endocardial borders using coupled active contours. In *Proc. Comput. Assisted Radiol. Surg.*, page 11471152.
- Thygesen, K., Alpert, J., White, H., and et.al. (2007). Universal definition of myocardial infarction. *European Heart Journal*, 28(20):2525–2538.
- Wei, D., Sun, Y., Chai, P., Low, A., and Ong, S. (2011). Myocardial segmentation of late gadolinium enhanced mr images by propagation of contours from cine mr images. *Med Image Comput Comput Assist Interv*, 14:428–35.
- Wei, D., Sun, Y., Ong, S., Chai, P., Teo, L. I., and Low, A. F. (2013). Three-dimensional segmentation of the left ventricle in late gadolinium enhanced mr images of chronic infarction combining long- and short-axis information. *Medical Image Analysis*, 17(6):685–697. doi:10.1016/j.media.2013.03.001.